Direct pericyte-to-neuron reprogramming via unfolding of a neural stem cell-like program

Marisa Karow [1,2,14]*, J. Gray Camp [3,14], Sven Falk[2,4], Tobias Gerber[3], Abhijeet Pataskar[5], Malgorzata Gac-Santel[3], Jorge Kageyama[3], Agnieska Brazovskaja[3], Angela Garding[5], Wenqiang Fan[1], Therese Riedemann [2], Antonella Casamassa[1,13], Andrej Smiyakin[6], Christian Schichor[7], Magdalena Götz [2,4], Vijay K. Tiwari[5], Barbara Treutlein [3,8,9,15]* and Benedikt Berninger [1,10,11,12,15]*

Ectopic expression of defined transcription factors can force direct cell-fate conversion from one lineage to another in the absence of cell division. Several transcription factor cocktails have enabled successful reprogramming of various somatic cell types into induced neurons (iNs) of distinct neurotransmitter phenotype. However, the nature of the intermediate states that drive the reprogramming trajectory toward distinct iN types is largely unknown. Here we show that successful direct reprogramming of adult human brain pericytes into functional iNs by Ascl1 and Sox2 encompasses transient activation of a neural stem cell-like gene expression program that precedes bifurcation into distinct neuronal lineages. During this transient state, key signaling components relevant for neural induction and neural stem cell maintenance are regulated by and functionally contribute to iN reprogramming and maturation. Thus, Ascl1- and Sox2-mediated reprogramming into a broad spectrum of iN types involves the unfolding of a developmental program via neural stem cell-like intermediates.

Direct lineage reprogramming is an emerging strategy for harnessing the cellular plasticity of differentiated cells for lineage conversion into desired target cell types for disease modeling and tissue repair[1–4]. While direct lineage reprogramming from starting to target-cell type classically occurs without cell division, thereby sharply contrasting with reprogramming toward induced pluripotency[5], little is known about the intermediate states that bridge the trajectory between start and end points. Two models have been proposed, according to which direct reprogramming is mediated either through direct conversion between fully differentiated states or through reversal to a developmentally immature state[6]. Furthermore, reprogramming efficiency and final differentiation outcomes are highly cellular-context-dependent, for which the underlying reasons are only incompletely understood[7,8]. Analyses of the transcriptome alterations induced by the reprogramming factors have yielded fundamental insights into the molecular mechanisms of iN conversion[9–12]. For instance, a single factor, Ascl1, can reprogram mouse astrocytes into iNs with high efficiency[13], while the same factor induces a muscle cell-like fate in mouse embryonic fibroblasts (MEF) alongside neuronal fates[11,14]. Efficient reprogramming of MEFs into iNs requires co-expression of additional factors (for example, Brn2, Ascl1 and Myt1l, collectively referred to as BAM)[9,11,12,15]. Moreover, Ascl1 induces a GABAergic neuron identity in mouse astrocytes[10,13], while BAM-transduced fibroblasts predominantly adopt a glutamatergic phenotype[15], raising questions

of how the respective reprogramming trajectories translate into distinct iN transmitter and subtype identities.

In the present study, by analyzing transcriptomes at population and single cell level, we aimed to reconstruct the trajectories underlying direct lineage conversion of adult human brain pericytes into iNs by forced expression of Ascl1 and Sox2 (AS)[16]. This allowed us to scrutinize the contribution of the starting cell population's heterogeneity to the variability in reprogramming success. By identifying cells of distinct reprogramming competence, we were able to reconstruct a trajectory of productive AS-mediated iN generation, allowing us to uncover intermediate states during successful conversion. Unexpectedly, we found that despite the absence of cell division, cells in the productive trajectory passed through a neural stem cell-like state. Transiently induced genes, many of which are core components of signaling pathways, typified this intermediate state, and interference with these signaling pathways demonstrated their functional importance for the reprogramming process. Finally, the productive reprogramming trajectory revealed an unexpected point of bifurcation into lineages whose transcriptomes were dominated by transcription factor families involved in the specification of GABAergic and glutamatergic subclasses of forebrain neurons.

Results

Ascl1 and Sox2 synergism in inducing neuronal gene expression in pericytes. We have recently shown that adult human brain

[1]Institute of Physiological Chemistry, University Medical Center Johannes Gutenberg University Mainz, Mainz, Germany. [2]Physiological Genomics, Biomedical Center, Ludwig Maximilians University Munich, Planegg/Martinsried, Germany. [3]Max Planck Institute for Evolutionary Anthropology, Leipzig, Germany. [4]Institute for Stem Cell Research, Helmholtz Center Munich, German Research Center for Environmental Health, Neuherberg, Germany. [5]Institute of Molecular Biology (IMB), Mainz, Germany. [6]Miltenyi Biotec GmbH, Bergisch Gladbach, Germany. [7]Department of Neurosurgery, Ludwig Maximilians University, Munich, Germany. [8]Max Planck Institute of Molecular Cell Biology and Genetics, Dresden, Germany. [9]Technical University Munich, Munich, Germany. [10]Focus Program Translational Neuroscience, Johannes Gutenberg University Mainz, Mainz, Germany. [11]Centre for Neurodevelopmental Biology, Institute of Psychiatry, Psychology & Neuroscience, King's College London, London, UK. [12]MRC Centre for Neurodevelopmental Disorders, King's College London, London, UK. [13]Present address: Division of Pharmacology, School of Medicine, "Federico II" University of Naples, Naples, Italy. [14]These authors contributed equally: Marisa Karow, J. Gray Camp. [15]These authors jointly supervised this work: Barbara Treutlein, Benedikt Berninger. *e-mail: marisa.karow@med.uni-muenchen.de; barbara_treutlein@eva.mpg.de; benedikt.berninger@kcl.ac.uk
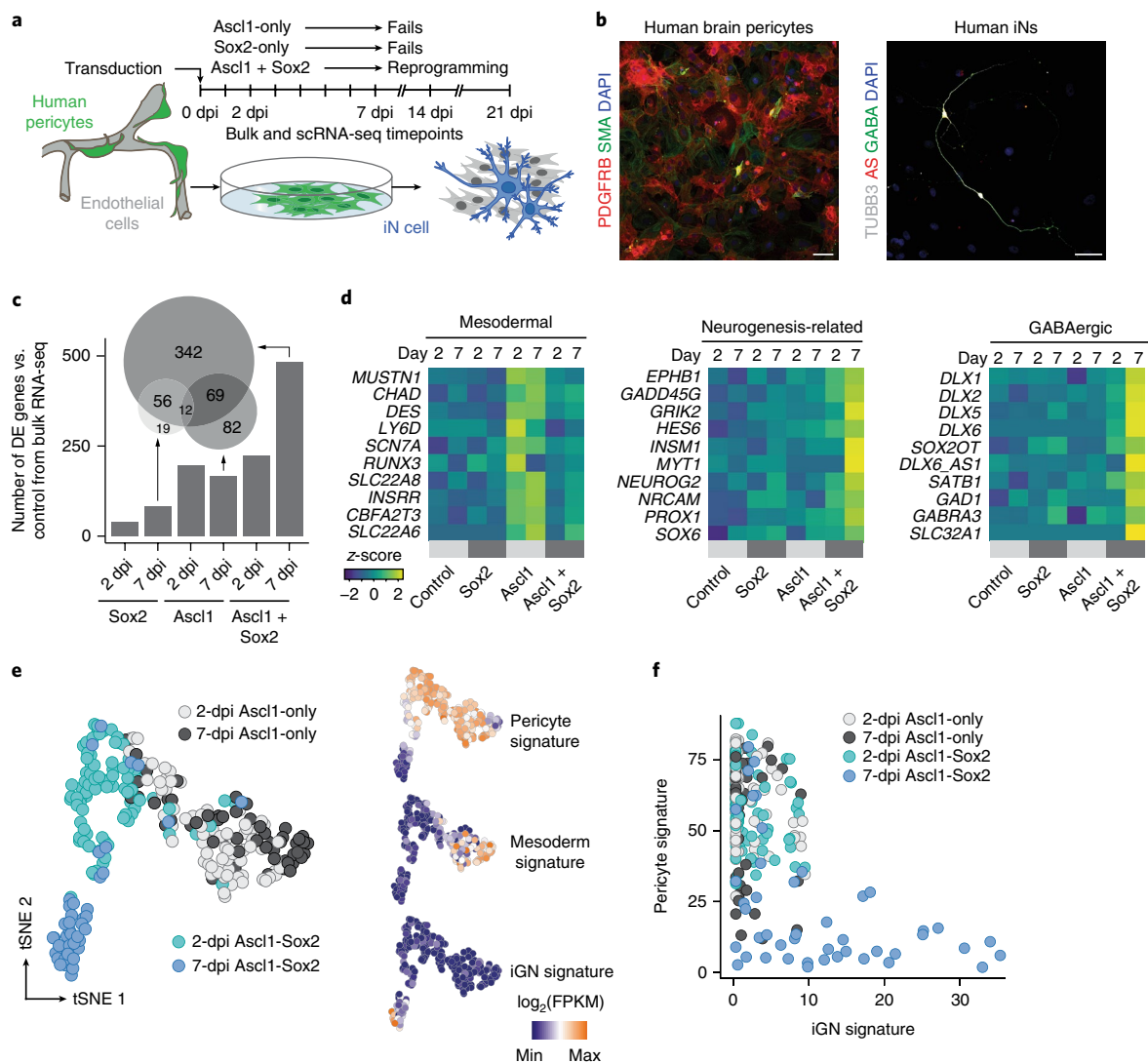
Fig. 1 | Ascl1–Sox2 synergism is required for pericyte-to-iN reprogramming. a, Schematic of experiments in this figure. Cells expressing Ascl1 and/or Sox2 are fluorescently labeled and isolated by fluorescence-activated cell-sorting (FACS) for bulk and scRNA-seq analyses at indicated timepoints following transduction. **b**, Representative micrographs of cultured human pericytes expressing pericyte markers PDGFRB and SMA, before (left) and after transformation (right) into TUBB3+ and GABA+ iNs by overexpressing AS at 46 dpi ($n > 30$). Nuclei are stained with DAPI. Scale bar, 50 µm. **c**, Bulk RNA-seq with pericytes derived from three individual donors was performed at 2 and 7 dpi with Ascl1-only, Sox2-only, or AS. Bar graph shows the number of differentially expressed (DE) genes (adjusted P value (P_{adj}) < 0.01; calculated according to Benjamini–Hochberg) in each condition compared to pericytes transduced with a control vector. The Euler diagram shows the overlap of the DE genes at 7 dpi. Note that the majority of DE genes results from AS synergism. **d**, Heatmaps show normalized expression (z-score) of representative DE genes highlighting the induction of mesodermal, neurogenesis-related, and GABAergic signature genes at both 2 and 7 dpi. **e**, scRNA-seq was performed at 2 and 7 dpi on cells transduced with Ascl1-only ($n = 82$ cells at 2 dpi and 64 cells at 7 dpi) and AS ($n = 86$ cells at 2 dpi and 48 cells at 7 dpi). Principal component analysis (PCA; calculated on a total of 280 cells) followed by t-SNE shows that the pericyte signature is diminished in many 7-dpi Ascl1-only and strongly diminished in the majority of 7-dpi AS cells, concomitant with the acquisition of a mesoderm and GABAergic neuron (iGN) signature in Ascl1-only and AS-cells, respectively. Signatures were calculated by summing the expression of the fate-determinants highlighted in **d** (Supplementary Table 5). **f**, The iGN signature is plotted for all Ascl1-only and AS cells relative to the pericyte signature.

pericytes can be reprogrammed into iNs via forced expression of the transcription factors Ascl1 and Sox2, and time-lapse imaging showed that this conversion occurs in the absence of cell division, qualifying it as direct lineage reprogramming[16]. Given that adult human brain pericyte reprogramming into functional iNs requires co-expression of Sox2 alongside Ascl1[16], we first addressed the contribution of each factor, individually or in combination, to the gene expression programs underlying pericyte-to-neuron conversion (Fig. 1a,b). We performed RNA-seq of early-passage cultured human brain pericytes, obtained from three different adult donors, and transduced them with retroviruses encoding a reporter for control, Ascl1, Sox2, or AS at early stages (2 d postinfection (dpi) and 7 dpi) of reprogramming (Fig. 1a). Unexpectedly, Sox2 only induced minor changes in gene expression, at both 2 and 7 dpi (Fig. 1c, Supplementary Fig. 1a,e, and Supplementary Table 1). In contrast, Ascl1 and AS substantially altered gene expression at both stages (Fig. 1c and Supplementary Fig. 1a,e,f). Notably, Ascl1 and AS changed the expression of distinct sets of genes. We noticed that several of the Ascl1-only altered genes are expressed in cells of the mesodermal lineage, indicative of a failure to cross the

lineage barrier toward neurogenesis. In sharp contrast, AS resulted in substantial induction of genes related to neurogenesis (Fig. 1d, and Supplementary Fig. 1e,f, and Supplementary Table 1). Moreover, we detected upregulation of several transcription factors and non-coding RNAs playing key roles in forebrain GABAergic neurogenesis[17,18] (Fig. 1d, Supplementary Fig. 1e,f, and Supplementary Tables 1 and 2). Yet we also observed a significant increase in *NEUROG2* expression (Fig. 1d), which is associated with diverse excitatory neuron identities.

Comparison of the genes upregulated by Ascl1-only or by AS with those transactivated by Ascl1 in mouse neural stem cells[19] revealed a progressive induction of direct Ascl1 neural stem cell target genes between 2 and 7 dpi (Supplementary Fig. 1b and Supplementary Table 3). However, many of the direct Ascl1 neural stem cell target genes became induced only upon co-expression of Sox2 (Supplementary Fig. 1c,d), indicating that the proposed on-target pioneer factor activity of Ascl1[9,19] is highly context-dependent.

To further dissect the differences in the early gene expression programs induced by Ascl1 or AS, we measured 280 single-cell transcriptomes of Ascl1- ($n = 146$) and AS-expressing ($n = 134$) cells by single-cell RNA-seq (scRNA-seq) at 2 and 7 dpi. Principal component analysis followed by t-stochastic neighbor embedding (t-SNE) of single-cell transcriptomes revealed an early and progressive separation of Ascl1-only and AS-expressing cells (Fig. 1e). Pericyte identity genes (for example, *PDGFRB*, *COL1A1*, and *CAV1*) became downregulated in Ascl1- and AS-expressing cells (Supplementary Fig. 1g), but only the latter acquired a GABAergic neuron fate signature (*DLX1/2*, *DLX5/6*, *SATB1*, etc.; Fig. 1e and Supplementary Fig. 1h). In agreement with our bulk RNA-seq data and published data from MEF-to-neuron reprogramming[11], Ascl1-expressing cells induced myocyte differentiation genes (for example, *MUSTN1*; Supplementary Fig. 1h). Occasionally, individual AS cell transcriptomes clustered with those of Ascl1-only cells, suggesting failed AS synergism as a potential mechanism underlying reprogramming failure (Fig. 1f). Overall, these data demonstrate that Ascl1 alone is unable to induce a neuronal program in adult human brain pericytes but requires synergism with Sox2.

Pericyte heterogeneity and reprogramming competence. To define the competence of adult human brain pericytes for AS-induced reprogramming, we next compared the transcriptomes of control pericytes with those of AS-transduced cells at early and later stages of reprogramming. To our surprise, t-SNE analysis revealed that control cells fell into two discernible clusters (Fig. 2a,b and Supplementary Fig. 2a,b), here referred to as group 1 and group 2 pericytes, with differentially enriched gene ontology terms (Supplementary Fig. 2c and Supplementary Table 4). While both groups highly expressed several classical pericyte genes (i.e., *PDGFRB*, *CAV1*, *DCN*, etc.; Fig. 2a and Supplementary Fig. 2b), other pericyte-associated genes such as *ANGPT1*, *APOE*, and *LEPR* were differentially expressed (Supplementary Fig. 2a,b), and such differential expression could be confirmed on the protein level (Fig. 2c,f and Supplementary Fig. 2d). Notably, transcriptomes of AS-transduced cells exhibited distinct degrees of relatedness to the two pericyte starting populations, with cells undergoing successful reprogramming being more similar to group 2 pericytes (Fig. 2d,e). These data strongly suggest that the two pericyte groups differed markedly in their response to AS. In fact, t-SNE analysis indicated that productive reprogramming toward neurogenesis originated specifically from group 2 pericytes (Fig. 2a,e). In contrast, group 1 pericytes appeared to give rise to a distinct population positive for the hypothalamic neuronal marker PMCH but lacking expression of other neuronal genes, which thus precluded identifying these cells as hypothalamic neurons (Fig. 2a). Besides AS-transduced cells clustering differentially with group 1 and group 2 pericytes, we observed two smaller clusters of AS-transduced cells enriched in

genes involved in cell-cycle progression (for example, *MKI67*) and potentially an alternative fate marked by the expression of *POU2F3*. To independently corroborate differential neurogenic competence of group 1 and group 2 pericytes, we used fluorescence-activated cell sorting to purify these populations via antibodies specific to the leptin receptor, encoded by the *LEPR* gene (Fig. 2f,g and Supplementary Fig. 2a,b). Consistent with the observation that iNs may originate from group 2 pericytes, we found that leptin-receptor-negative cells were more prone to undergo AS-induced neurogenesis than leptin-receptor-positive cells (Fig. 2h). These data provide experimental evidence that the two pericyte starter populations display distinct degrees of reprogramming competence.

Transient activation of a neural stem cell-like program. We next reconstructed the transcriptome trajectory of reprogramming-competent pericytes into iNs by pseudotemporal ordering[20] (Fig. 3a). Genes that mark pericyte identity, such as *PDGFRB*, *CAV1*, and *CFH*, became gradually downregulated. Conversely, genes associated with the acquisition of a neuronal fate were progressively upregulated with more linear (for example, *CHD7* and *DLX5*) or nonlinear dynamics (for example, *SNAP25*; Fig. 3b,c), possibly reflecting distinct gene expression waves during early and later phases of neuronal differentiation. Notably, we identified a set of genes that became upregulated early during the reprogramming process, but then declined again as neuronal differentiation progressed (Fig. 3b,c). We refer to these genes as 'switch genes'. These include genes involved in the regulation of cell signaling such as *NOG*, *LEFTY2*, *DKK1*, and *NOTCH2*, suggesting that modulation of signaling pathways is important during early phases of productive reprogramming (see below). The conspicuous dynamics of the regulation of these genes urged us to interrogate their expression during mouse embryonic development. Notably, the switch genes were markedly enriched in the germinal zones of the developing CNS containing the neural stem cells (Fig. 3d and Supplementary Fig. 3a). This strongly suggests that cells undergoing productive reprogramming by AS transiently acquire a neural stem cell-like state. This was further corroborated when analyzing the expression levels of these genes in human fetal brain tissue[21], where higher levels of expression were found in distinct human neural stem cells (i.e., apical and basal radial glia) as compared to neurons (Fig. 3e). Consistent with the upregulation of the switch genes during successful reprogramming, mapping the switch gene signature onto the t-SNE plot shown in Fig. 2a revealed its specific occurrence in the cell population that connects productive group 2 pericytes with iNs (Fig. 3f). In contrast, the switch gene signature was absent from transcriptomes of AS-transduced cells in the immediate neighborhood of group 1 pericytes (Fig. 3f), indicating that acquisition of a neural stem cell like-state is critical for AS-mediated pericyte-to-iN reprogramming. Of note, mapping the same switch gene signature onto previously published single-cell transcriptomes undergoing MEF-to-iN reprogramming[11] revealed an unexpectedly high base level of switch gene expression in the MEF starting population, and its expression did not increase at any stage along the MEF-to-neuron axis but was found to be strongly decreased in neurons (Supplementary Fig. 3b). These data are indicative of fundamental differences in the reprogramming trajectories of these two distinct reprogramming pathways. Notably, time-lapse imaging of pericytes during AS reprogramming revealed the occurrence of different cellular morphologies: while at early phases of reprogramming, cells displayed a flat, fibroblast-like morphology, at subsequent phases, processes undergoing dynamic turnover akin to multipolar progenitors appeared (Fig. 3g and Supplementary Video 1). Finally, at the end of the reprogramming process, neuron-like cells dramatically decreased their motility and protruded processes of increased stability. Thus, the cellular behavior and morphology are consistent with the notion of distinct cellular states underlying the reprogramming of pericytes into iNs.
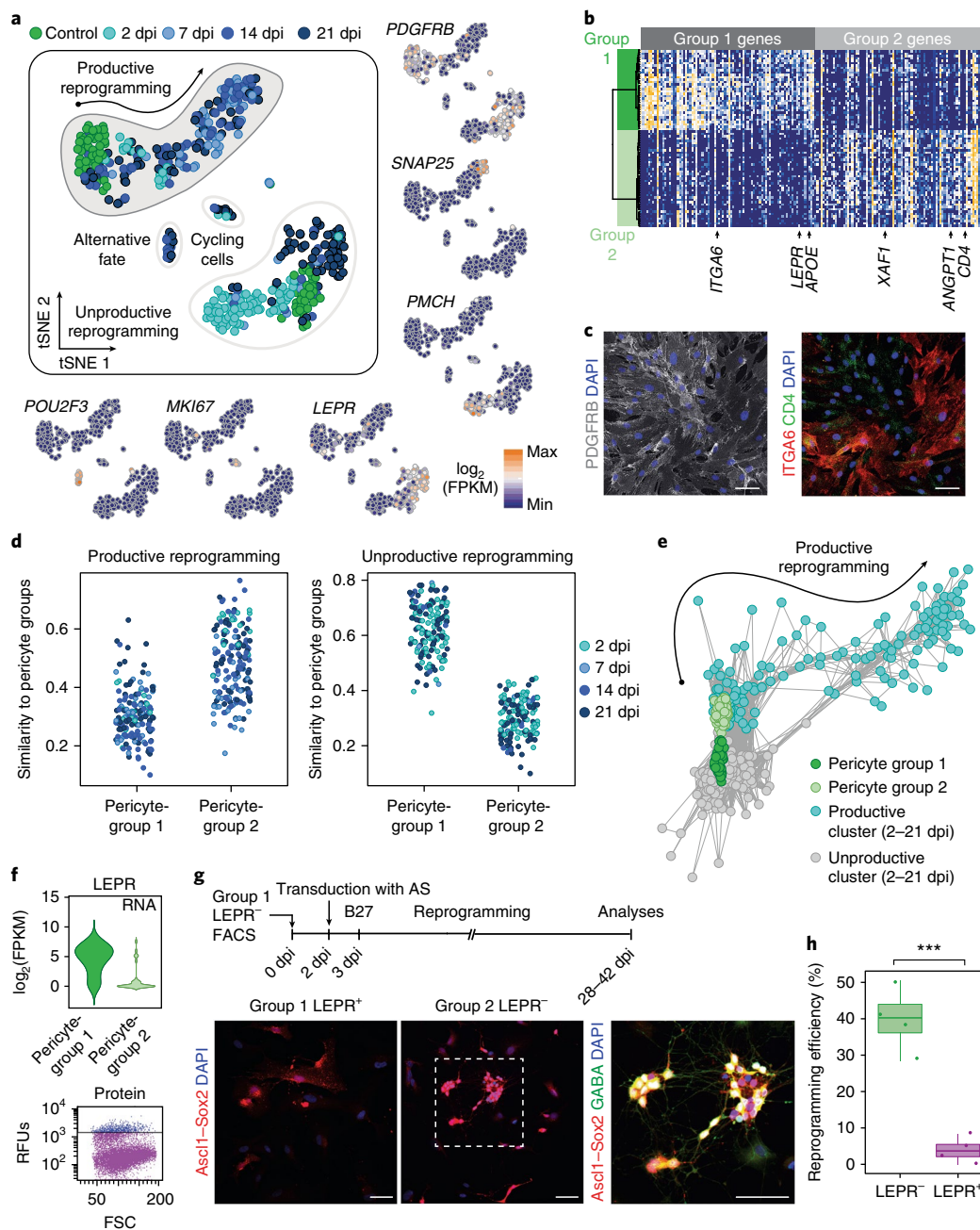
Fig. 2 | Pericyte heterogeneity correlates with distinct reprogramming competence. a, PCA (total of 419 cells) followed by t-SNE reveals heterogeneity during iN reprogramming, with genes marking distinct clusters colored on the adjacent t-SNE plots. Control-transduced pericytes (green) segregate into two distinct clusters. One cluster links to cells that express iN fate determinants (productive), whereas the other cluster is unlinked to iN reprogramming (unproductive). Cells expressing *MKI67* and other hallmarks of cycling cells are observed, as well as a group of cells expressing *POU2F3*. **b**, Heatmap shows the expression of genes that correlate with PC1 from PCA on control pericytes only. Hierarchical clustering reveals two distinct groups of pericytes with selected genes indicated below the heatmap. **c**, Left: micrographs showing cultured human brain pericytes stained against the pan-pericyte marker PDGFRB. Right: the same field of view of cultured human brain pericytes stained against pericyte group 1 marker ITGA6 and pericyte group 2 marker CD4. Nuclei are stained with DAPI (*n* = 3 individual pericyte donors; two independent experiments). Scale bar, 50 μm. **d**, Cells from the productive reprogramming cluster in **a** have a higher similarity to group 2 pericytes, while cells from the unproductive reprogramming clusters have a higher similarity to group 1 pericytes. **e**, Lineage network based on pairwise correlations between cells suggests that group 2 pericytes (lighter green population) are more competent to contribute to productive iN reprogramming. **f**, Top: violin blots show the density distribution of RNA expression of *LEPR* in pericyte groups 1 (31 cells) and 2 (44 cells). Bottom: representative flow cytometry plots show LEPR expression in cultured human brain pericytes (four independent experiments). RFUs, relative fluorescence units; FSC, forward scatter signal. **g**, Human brain pericytes were sorted based on LEPR expression (group 1 marker), plated, and transduced with AS to induce lineage conversion. Micrographs show AS-transduced pericytes at 35 dpi, with inset showing higher magnification of reprogrammed pericytes that acquired neuronal morphology and GABA immunoreactivity (*n* = 4). Nuclei are stained with DAPI. Scale bars, 50 μm. **h**, Quantification of reprogramming efficiency (dots represent independent individual experiments; *n* = 4; data are represented as boxplots with whiskers; two-tailed unpaired Student's *t* test; ***P = 0.000593) reveals that the LEPR⁻ pericyte subpopulation is more competent to iN reprograming using AS, confirming predictions from scRNA-seq. Boxplots show median, quartiles (box), and range (whiskers).

Modulation of signaling pathways. The conspicuous regulation of several components of signaling pathways known to play key roles during neural induction and neural stem cell maintenance[22], such as the BMP inhibitor NOG, the ACTIVIN/NODAL inhibitor LEFTY2, and NOTCH2 and its downstream targets HEY1 and ID1, prompted us to investigate whether these pathways are of functional importance for successful reprogramming. To test the importance of modulation of NODAL and BMP signaling, we treated pericytes during early phases of reprogramming with recombinant NODAL (1 µg/mL) and BMP4 (30 ng/mL; Fig. 4a,b). These treatments resulted in a significant reduction of reprogramming as determined by the number of TUBB3+ cells amongst AS-transduced cells (Fig. 4c). Conversely, inhibition of BMP, ACTIVIN/NODAL, and TGF-β signaling via the small molecules dorsomorphin (1 µM) and SB431542 (10 µM) caused a threefold increase in the number of reprogrammed iNs (Fig. 4d,e). To address the relevance of NOTCH signaling in the reprogramming process, we treated AS-transduced pericytes with the γ-secretase inhibitor N-[N-(3,5-difluorophenacetyl)-L-alanyl]-S-phenylglycine t-butyl ester (DAPT). DAPT treatment (10 µM) resulted in a marked increase in the number of iNs (Fig. 4d,e). This finding is consistent with the role of NOTCH signaling in neurogenesis inhibition and neural stem cell maintenance[23].

Though AS induction leads to productive iN reprogramming, we observed that maturation seemed to stall at 14 dpi, either because cells at later timepoints failed to mature further or because of a technical bias against harvesting healthy iNs at later stages (Fig. 3a). Our data showed that productive reprogramming involved inhibition of BMP signaling, and blocking BMP signaling appeared to promote maturation, as suggested by increased morphological iN complexity (Fig. 4e). We therefore analyzed the effect of the BMP inhibitor dorsomorphin during early phases of the reprogramming process on subsequent neuronal maturation (Fig. 5a). Dorsomorphin-treated AS-induced neurons exhibited markedly increased morphological complexity and soma size (Fig. 5b,c and Supplementary Fig. 4a), as well as increased membrane capacitance and decreased membrane resistance (Fig. 5d and Supplementary Fig. 4b). scRNA-seq on dorsomorphin-treated AS-induced neurons revealed that genes associated with synapse formation and synaptic function showed increased expression relative to untreated AS-transduced cells (Fig. 5e). In line with enhanced iN maturation, we also noted enhanced GABA and PVALB immunoreactivity (Supplementary Fig. 4c).

Bifurcation into distinct iN lineages. These data prompted us to have a closer look at the neuronal subtype specification induced by AS with or without dorsomorphin (ASD). We focused on iNs that expressed both *SNAP25* and *MAP2* and analyzed 20 AS and 72 ASD cells. The majority of AS and ASD iNs exhibited a forebrain GABAergic interneuron program characterized by coordinated expression of multiple members of the *DLX* gene family (Fig. 5f). Notably, we found evidence for further subspecification among the *DLX*-expressing iNs. We observed distinct clusters of *VIP*-expressing neurons, some of which also co-expressed *CCK*. Likewise, we noted two clusters specifically expressing *SST* (Fig. 5f).

However, we also noted a subset of iNs that expressed a transcription factor of the glutamatergic lineage, *NEUROG2*. Notably, these iNs also expressed downstream targets *NEUROD1* and *NEUROD4*, consistent with the expression of a telencephalic glutamatergic neuron program[10,24]. The fact that this subset also expressed *RELN* (Fig. 5f) may indicate that these iNs acquire a Cajal–Retzius neuron-like program. It is noteworthy that, while the majority of *DLX1*-expressing cells were NEUROG2− and many high-NEUROG2+ cells were DLX1−, we observed some outliers expressing both genes (Supplementary Fig. 4d). This may reflect the possibility that the definitive decision between the two major neuron lineages (GABA versus glutamate) had not yet taken place in these cells. To reveal the developmental trajectory toward a *DLX*- or *NEUROG2*-dominated

fate, we employed pseudotemporal ordering of the transcriptomes of AS cells of the productive path and 14-dpi ASD cells. Notably, we observed a bifurcation of the trajectory into *DLX*- or *NEUROG2*-dominated pathways, which preceded neuronal differentiation marked by *SNAP25* expression (Fig. 5g and Supplementary Fig. 4e). Projecting the switch gene signature identified in Fig. 3c onto the reprogramming path revealed that the transient expression of neural stem cell-like genes occurred and ceased before lineage bifurcation (Fig. 5h). Consistent with the increased maturation of ASD cells, the distribution of ASD transcriptomes was shifted farther along the trajectory of pericyte-to-iN reprogramming (Fig. 5i). We corroborated the emergence of *DLX*- or *NEUROG2*-expressing inhibitory and excitatory neuronal lineages using an alternative scRNA-seq method and a second pericyte donor (Supplementary Fig. 5).

To test whether NEUROG2 indeed suffices to induce a glutamatergic phenotype, we overexpressed *Neurog2* alongside AS (Supplementary Fig. 4f). *NEUROG2* overexpression resulted in the almost complete suppression of *DLX2* (Fig. 5j), suggesting that NEUROG2 can divert iNs from adopting predominantly a GABAergic phenotype toward generating mostly glutamatergic neurons. Accordingly, we found that *NEUROG2*-overexpressing AS neurons exhibited vesicular glutamate transporter immunoreactivity (Supplementary Fig. 4g).

Discussion

Here we have shown that reprogramming success of adult human brain pericytes into iNs by the transcription factors Ascl1 and Sox2 (AS) critically depends on cellular context, as revealed by the observation that pericyte heterogeneity is a key determinant for reprogramming competence. Successful reprogramming by AS encompasses the passage through a neural stem cell-like intermediate state, yet it occurs in the absence of cell division. Moreover, regulation of signaling pathways during the neural stem cell-like state was of functional importance for the reprogramming outcome. This data indicates that AS-mediated reprogramming involves the unfolding of developmental programs and argues for the engagement of hierarchical developmental gene-regulatory networks[6] rather than direct interconversion between two states of terminal differentiation. Finally, we found that, following the transition through a neural stem cell-like state, the reprogramming trajectory eventually bifurcates to give rise to two distinct branches characterized by *DLX*- or *NEUROG*-dominated gene expression and indicative of bifurcation into GABAergic or glutamatergic lineages, respectively. This provides a mechanistic explanation for the common observation that a single reprogramming cocktail can yield neurons of distinct neurotransmitter phenotypes[15,25].

We observed that the reprogramming competence of adult human brain pericytes is highly variable and a main source for this variability is pericyte heterogeneity. Heterogeneity of pericytes has been described in many tissues and may reflect distinct embryonic origins[26]. Our scRNA-seq experiments revealed two distinct populations, one of which, characterized by high *LEPR* expression, displayed markedly reduced reprogramming propensity. Notably, a recent study using scRNA-seq showed that several of the heterogeneously expressed genes are also expressed at highly variable levels in acutely isolated human midbrain pericytes[27], which might indicate that similar heterogeneity occurs in vivo. However, our study may actually underestimate overall pericyte heterogeneity, as we included in our scRNA-seq analysis only retrovirus-transduced cells, for which ongoing cell division at the time of transduction is required. We would also expect that proliferative pericytes do not perfectly match pericytes under resting conditions, but may be more akin to those found to undergo cell division in response to severe CNS injury[28].

Revealing the cell-context requirements for reprogramming is of greatest importance if direct lineage reprogramming is to be of
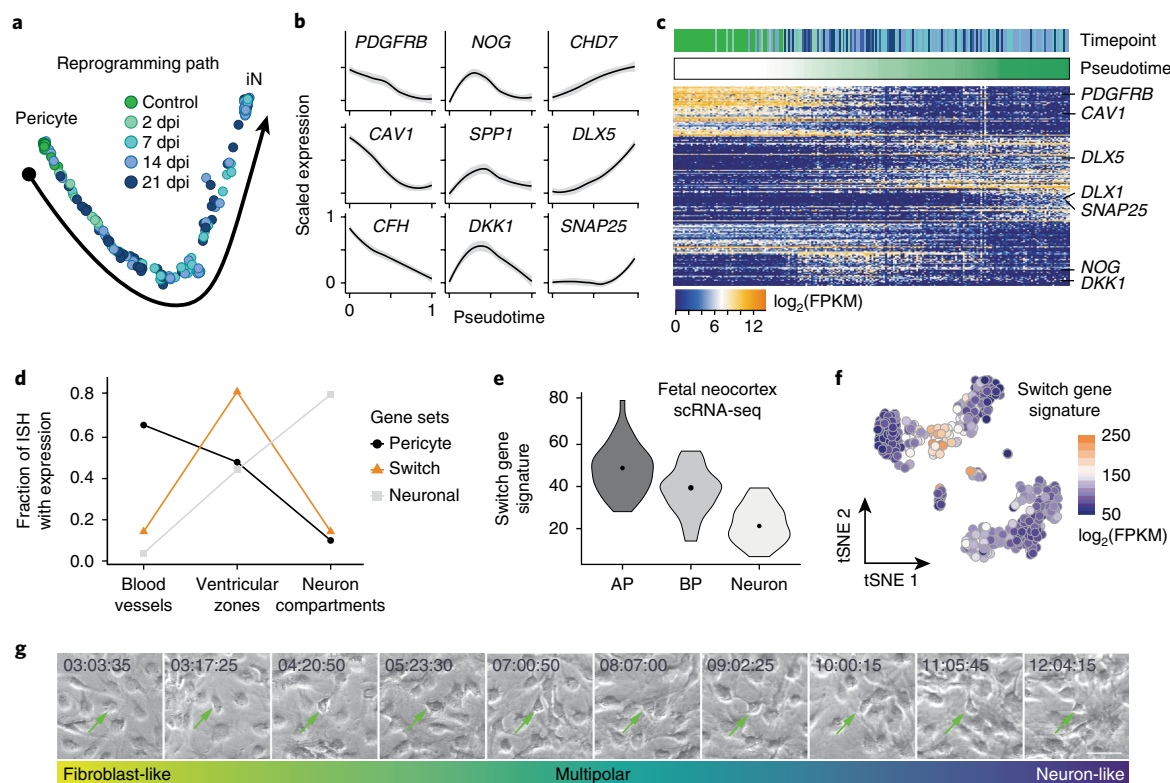
Fig. 3 | A transient neural precursor-like state emerges on the reprogramming path to iNs. a, PCA was performed on 211 single-cell transcriptomes from the productive reprogramming cluster shown in Fig. 2a. Monocle2 was used to infer a pseudotemporal ordering of cells. **b**, Scaled expression of representative marker genes in all 211 cells of the productive reprogramming path shown as a function of pseudotime. Shaded gray represents 95% confidence interval. **c**, Heatmap shows the expression of genes identified by PCA and ordered by hierarchical clustering. Cells are ordered according to pseudotime. The reprogramming path is characterized by three phases of gene expression changes. In the first phase, genes associated with pericyte identity are downregulated, concomitant with a transient upregulation of switch genes (for example, *NOG* and *DKK1*). In the second phase, genes associated with iN fate determination are upregulated (for example, *DLX5*). In the third phase, neuron maturation factors (for example, *DLX1* and *SNAP25*) are upregulated alongside phase 2 genes. **d**, Chart shows fraction of pericyte, switch, and neuronal genes (from **c**) expressed in blood vessels and meninges, ventricular zones, or neuron compartments determined from in situ patterns in the developing mouse brain. ISH, in situ hybridization. **e**, Violin plots show the density distribution of the switch gene signature from scRNA-seq of fetal human cortex (dots within the violins represent medians). Cortex cells are grouped based on cell type (41 apical progenitor cells (AP); 19 basal progenitor cells (BP); 42 early-born neurons (Neuron)). **f**, Switch gene signatures projected onto the t-SNE plot from Fig. 2a shows the induction of switch genes at an intermediate stage exclusively within the productive reprogramming path. **g**, Time-lapse imaging of AS-transduced cells over time (three independent experiments) shows the morphological changes during successful pericyte-to-neuron reprogramming (timepoints specified within the images). Arrows indicate a successfully reprogrammed pericyte throughout the different morphological changes mentioned below the images. Scale bar, 50 μm.

therapeutic value. Many reprogramming-factor cocktails that work well with mouse cells (for example, MEFs) are rather inefficient with human cells, and in particular, when the cells are of adult-tissue origin. It will be therefore a fruitful field of investigation to identify, in addition to transcriptome differences, epigenetic disparities between the two subpopulations of pericytes identified here. This may yield potential molecular targets for improved reprogramming strategies that may apply to other adult human somatic cell types.

A key finding of our study is the observation that AS-transduced cells pass through a neural stem cell-like state before differentiating into iNs. This neural stem cell-like state is characterized by expression of a battery of genes that are normally expressed in neural stem cells or progenitor cells during forebrain embryonic development, referred to here as switch genes as they are dynamically regulated during the reprogramming process. While referring to the state characterized by switch gene expression as a neural stem cell-like state, we do not equate it to a bona fide neural stem cell state. This distinction is warranted given the absence of classical markers of neural stem cells such as *MSI1* (Musashi) or *NES* (Nestin) during the switch state, some anomalies in gene

regulation such as *DLX5* expression preceding *DLX1* expression in time, and above all the absence of cell division and of a transcriptomic signature of an active cell cycle. We hypothesize that genes induced during the switch state represent a neural stem cell gene-expression module specifically regulated by Ascl1 and Sox2 and that other transcription factors may be required to induce other neural stem cell markers. Notably, the AS-induced neural stem cell expression module appears to be sufficient to drive the trajectory toward neuronal differentiation.

Switch genes include components of several signaling pathways, such as the ACTIVIN/NODAL (*LEFTY2*), BMP (*NOG*), and NOTCH (*HES5*, *HEY1*, *ID1*, *NOTCH2*) signaling pathways. By activating or inhibiting the ACTIVIN/NODAL and BMP pathways during the early phase of reprogramming through recombinant ligands or pharmacologically, we showed that these pathways exert an important influence on reprogramming efficiency. The fact that inhibition of ACTIVIN/NODAL and BMP signaling is required for reprogramming is consistent with the fact that inhibition of these pathways is important for neural induction during embryonic development[22], can be used for driving human
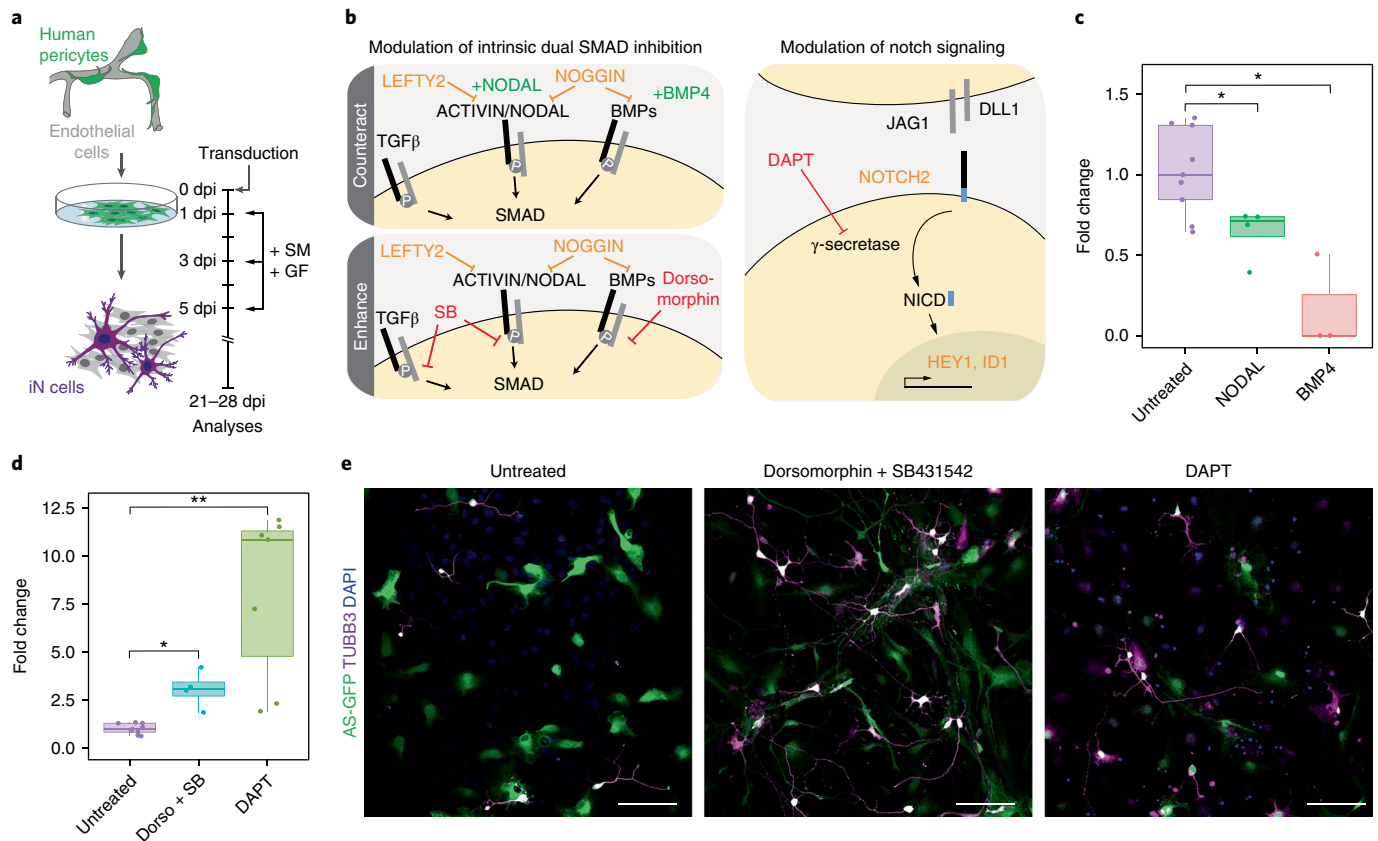
Fig. 4 | Modulation of signaling pathways identified during neural stem cell-like state. a, Schematic overview of the timeline for the experiments contained in this figure. Cells were treated with either small molecules (SM) or growth factors (GF). **b,** Schematic overview of switch gene expression associated with signaling pathways and summary of treatments. P, receptor phosphorylation induced by respective ligands. **c,** Treatment with NODAL or BMP4 decreases the reprogramming efficiency. Reprogramming efficiency was calculated by quantifying TUBB3-immunoreactive cells among reporter-positive transduced cells 3–5 weeks after transduction with AS. Fold-changes were calculated by determining the ratio of growth-factor-treated vs. nontreated TUBB3+Reporter+ cells per total Reporter+ cells of the transduced pericytes (dots represent independent individual experiments; untreated, $n=9$; NODAL, $n=4$; BMP, $n=3$; data are represented as boxplots with whiskers; two-tailed unpaired Student's t test; $P=0.01202$ for NODAL; $P=0.01821$ for BMP4; *$P<0.05$). Boxplots show median, quartiles (box), and range (whiskers). **d,** Reprogramming efficiencies (TUBB3+Reporter+ cells per total Reporter+ cells) increase following enhancing treatments with dorsomorphin (dorso) + SB431542 (SB) or DAPT. The fold change was calculated by determining the ratio of small-molecule-treated vs. nontreated TUBB3+Reporter+ cells per total Reporter+ cells of the transduced pericytes (dots represent independent individual experiments; untreated, $n=9$; dorso + SB, $n=4$; DAPT, $n=7$; data are represented as boxplots with whiskers; two-tailed unpaired Student's t test; *$P=0.02133$ for dorso + SB; **$P=0.0050$ for DAPT). Boxplots show median, quartiles (box), and range (whiskers). **e,** Representative micrographs of AS-transduced pericyte cultures (green) and stained with anti-TUBB3 (magenta). Note the increased appearance of reprogrammed pericytes that acquired neuronal morphology following dorso + SB ($n=4$) and DAPT ($n=7$) treatment compared to the untreated cells. Nuclei are stained with DAPI. Scale bars, 50 μm.

pluripotent stem cells toward neural lineages[29], and enhances transcription factor-mediated reprogramming[25,30]. Crucially, we found that inhibition of NOTCH signaling promoted reprogramming. This is consistent with the role of NOTCH signaling in preventing neuronal differentiation of neural stem cells[31]. The conspicuous induction of the NOTCH ligand DLL1 during reprogramming suggests that DLL1+ cells exert a differentiation inhibitory effect on other AS-transduced cells, an inhibition that can be relieved pharmacologically. Notably, iNs appear to express Myt1, which has recently reported to be induced cell-autonomously by Ascl1 and to repress Notch signaling[32]. Likewise, its close relative Myt1l, a widely used component of the BAM reprogramming cocktail, has been shown to repress Notch signaling[12]. This suggests that the BAM cocktail exhibits similarities to AS' mechanism of reprogramming, but that the addition of the postmitotic repressor Myt1l serves to curtail molecular pathways of the switch state that keep neuronal differentiation in check. Another intriguing aspect of *NOTCH2* expression during reprogramming is the fact

that Notch2 has been recently found to repress cell cycle-related genes and drive neural stem cells to quiescence, which may account in part for the lack of cell division during the switch state[33].

Unexpectedly, we found that human brain pericytes reprogrammed by AS bifurcate into lineages dominated by transcription factors that specify inhibitory and excitatory neuron fates. This bifurcation was corroborated using two distinct scRNA-seq platforms (Fluidigm C1 and 10×Genomics). While the *DLX* gene family-dominated branch was enriched for genes characteristic of GABAergic neuron lineage (for example, *GAD1* and *GAD2*), the *NEUROG*-expressing branch expressed other transcription factors characteristic of the glutamatergic neuron lineage, such as *NEUROD1* and *NEUROD4*. Moreover, cells of the latter lineage also expressed *RELN*, suggesting similarities to the Cajal–Retzius subtype of glutamatergic neurons. The fact that forced expression of *Neurog2* in AS-transduced pericytes suppresses *DLX* gene expression may indicate that lineage bifurcation is driven by mutual cross-repression of *NEUROG* and *DLX* family genes. Our
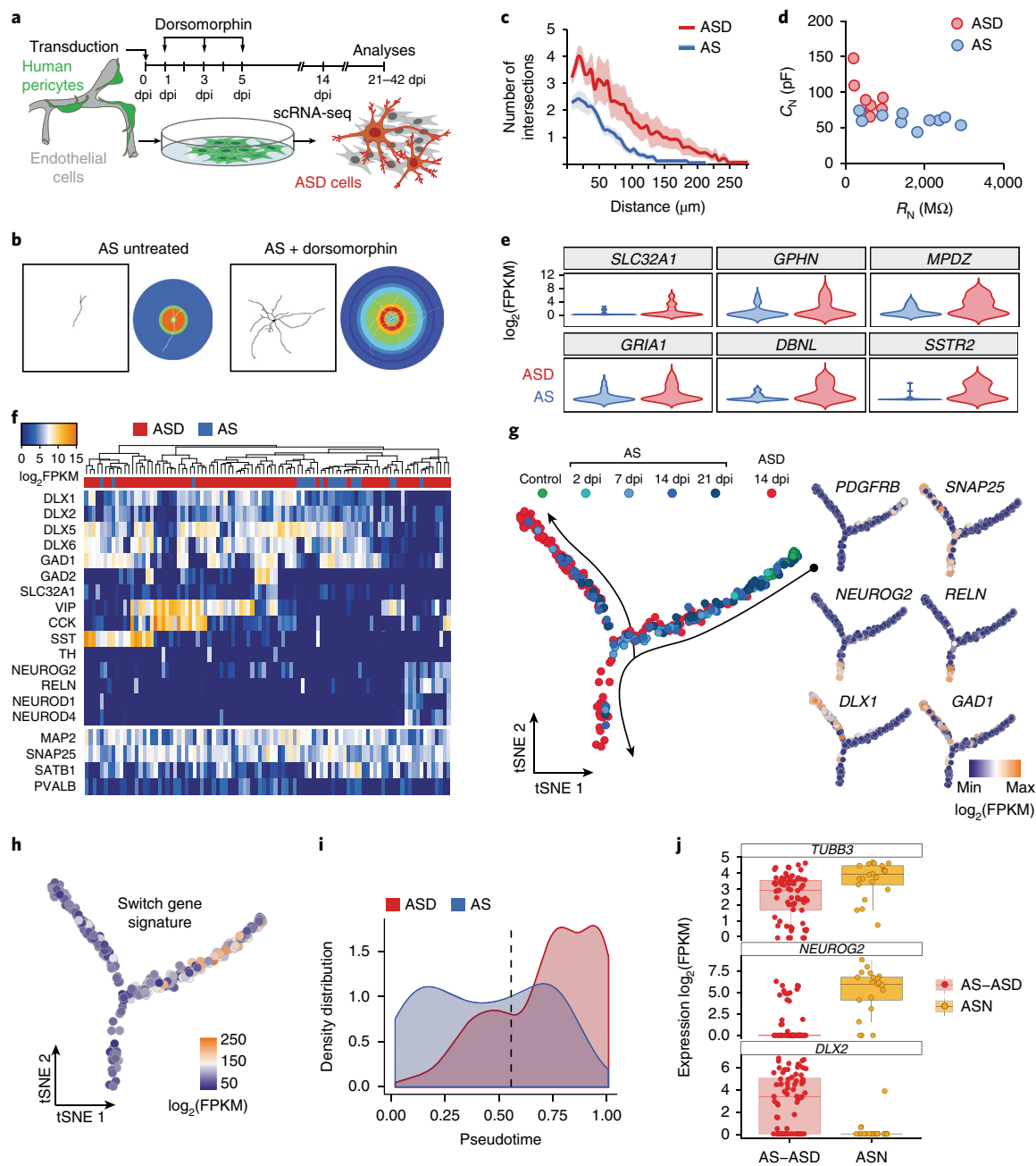
Fig. 5 | Pericytes give rise to distinct neuronal subtypes, and targeting BMP signaling promotes maturation. a, Schematic overview of experiments in this figure. **b**, Representative examples of untreated and dorsomorphin-treated AS-transduced pericytes showing complex branching of dendritic arbors in dorsomorphin-treated cells. Neuronal morphology was reconstructed using TUBB3 immunoreactivity and used for Sholl analyses. In the Sholl masks (right), warmer hues indicate higher number of intersections (untreated, $n = 14$ cells from 3 independent experiments; dorsomorphin-treated, $n = 14$ cells from 3 independent experiments). **c**, Single-cell neuromorphology reconstruction by Sholl analysis on dorsomorphin treated AS-transduced cells was compared to untreated cells. Note the increase in complexity of dorsomorphin-treated cells, which display more intersections with concentric shells and an overall increase in the length of the dendrites (see also Supplementary Fig. 4a). Data are represented in a line graph as mean ± s.e.m. (shaded region) (untreated, $n = 14$ cells from 3 independent experiments; dorsomorphin-treated, $n = 14$ cells from 3 independent experiments). **d**, Electrophysiological assessment of AS and ASD cells. Membrane capacitance (C_N) is plotted as a function of the membrane resistance (R_N). AS cells have greater R_N but smaller C_N compared to ASD cells. **e**, Violin blots show the density distribution of expression of selected neuronal maturation genes in neuronal (SNAP25+, MAP2+, PDGFRB−) AS cells ($n = 20$) and ASD cells ($n = 75$). **f**, PCA followed by hierarchical clustering was used to characterize neuronal cells (SNAP25+, MAP2+, PDGFRB−) AS cells ($n = 20$) and ASD cells ($n = 75$) at 14 dpi according to their expression of neuronal genes. Note the different interneuron clusters marked by the expression of interneuron subtype-specific genes *VIP*, *SST*, and *CCK*. **g**, Monocle2 was used to compare maturation of AS and ASD cells. **h**, Switch gene signature from Fig. 3c projected onto pseudotemporal ordered transcriptomes from **g**. **i**, The density distributions (i.e., normalized cell numbers per timepoint of pseudotime) along the pseudotime of AS transcriptomes (14 dpi) from the productive path and ASD transcriptomes (from **g**) are plotted as a function of the distance from the start point. Note the shift of ASD cell transcriptomes compared to AS transcriptomes. The dotted line indicates the bifurcation point in **g**. **j**, Jitter-boxplot (boxplots show median, quartiles (box), and range (whiskers)) showing the expression of *TUBB3* in all SNAP25+, MAP2+, PDGFRB− AS and ASD ($n = 71$), and AS + overexpressed *NEUROG2* (ASN; $n = 21$) cells used for this analysis. Boxplots show the strong increase of *NEUROG2* and decrease in *DLX2* gene expression in ASN cells as compared to AS and ASD cells.

data raise the intriguing possibility that the bipotent neural stem cell-like state observed during AS reprogramming relates to the suggested common precursor generating both glutamatergic and GABAergic neurons in the cerebral cortexes of human and nonhuman primates[34].

Overall, our study not only provides new insights into the biology underlying iN reprogramming, but also sheds light on the capacity of two transcription factors, Ascl1 and Sox2, to cooperate in the generation of diverse neuronal subtypes, a cooperation that may be relevant during human brain development. The identification of molecular programs that establish cellular intermediates and lineage bifurcations during iN reprogramming provides avenues for improving lineage conversion of human brain-resident cells toward therapeutically relevant cell types.

Methods

Methods, including statements of data availability and any associated accession codes and references, are available at https://doi.org/10.1038/s41593-018-0168-3.

References

1. Heinrich, C., Spagnoli, F. M. & Berninger, B. In vivo reprogramming for tissue repair. *Nat. Cell Biol.* **17**, 204–211 (2015).
2. Amamoto, R. & Arlotta, P. Development-inspired reprogramming of the mammalian central nervous system. *Science* **343**, 1239882 (2014).
3. Mertens, J., Marchetto, M. C., Bardy, C. & Gage, F. H. Evaluating cell reprogramming, differentiation and conversion technologies in neuroscience. *Nat. Rev. Neurosci.* **17**, 424–437 (2016).
4. Srivastava, D. & DeWitt, N. In vivo cellular reprogramming: the next generation. *Cell* **166**, 1386–1396 (2016).
5. Ruiz, S. et al. A high proliferation rate is required for cell reprogramming and maintenance of human embryonic stem cell identity. *Curr. Biol.* **21**, 45–52 (2011).
6. Morris, S. A. Direct lineage reprogramming via pioneer factors; a detour through developmental gene regulatory networks. *Development* **143**, 2696–2705 (2016).
7. Vierbuchen, T. & Wernig, M. Molecular roadblocks for cellular reprogramming. *Mol. Cell* **47**, 827–838 (2012).
8. Gascón, S., Masserdotti, G., Russo, G. L. & Götz, M. Direct neuronal reprogramming: achievements, hurdles, and new roads to success. *Cell Stem Cell* **21**, 18–34 (2017).
9. Wapinski, O. L. et al. Hierarchical mechanisms for direct reprogramming of fibroblasts to neurons. *Cell* **155**, 621–635 (2013).
10. Masserdotti, G. et al. Transcriptional mechanisms of proneural factors and REST in regulating neuronal reprogramming of astrocytes. *Cell Stem Cell* **17**, 74–88 (2015).
11. Treutlein, B. et al. Dissecting direct reprogramming from fibroblast to neuron using single-cell RNA-seq. *Nature* **534**, 391–395 (2016).
12. Mall, M. et al. Myt1l safeguards neuronal identity by actively repressing many non-neuronal fates. *Nature* **544**, 245–249 (2017).
13. Heinrich, C. et al. Directing astroglia from the cerebral cortex into subtype specific functional neurons. *PLoS Biol.* **8**, e1000373 (2010).
14. Chanda, S., Marro, S., Wernig, M. & Südhof, T. C. Neurons generated by direct conversion of fibroblasts reproduce synaptic phenotype caused by autism-associated neuroligin-3 mutation. *Proc. Natl. Acad. Sci. USA* **110**, 16622–16627 (2013).
15. Vierbuchen, T. et al. Direct conversion of fibroblasts to functional neurons by defined factors. *Nature* **463**, 1035–1041 (2010).
16. Karow, M. et al. Reprogramming of pericyte-derived cells of the adult human brain into induced neuronal cells. *Cell Stem Cell* **11**, 471–476 (2012).
17. Long, J. E. et al. Dlx1&2 and Mash1 transcription factors control striatal patterning and differentiation through parallel and overlapping pathways. *J. Comp. Neurol.* **512**, 556–572 (2009).
18. Liu, S. J. et al. Single-cell analysis of long non-coding RNAs in the developing human neocortex. *Genome Biol.* **17**, 67 (2016).
19. Raposo, A.A. et al. Ascl1 coordinately regulates gene expression and the chromatin landscape during neurogenesis. *Cell Rep.* https://doi.org/10.1016/j.celrep.2015.02.025 (2015).
20. Trapnell, C. et al. The dynamics and regulators of cell fate decisions are revealed by pseudotemporal ordering of single cells. *Nat. Biotechnol.* **32**, 381–386 (2014).
21. Camp, J. G. et al. Human cerebral organoids recapitulate gene expression programs of fetal neocortex development. *Proc. Natl. Acad. Sci. USA* **112**, 15672–15677 (2015).
22. Suzuki, I. K. & Vanderhaeghen, P. Is this a brain which I see before me? Modeling human neural development with pluripotent stem cells. *Development* **142**, 3138–3150 (2015).
23. Imayoshi, I., Sakamoto, M., Yamaguchi, M., Mori, K. & Kageyama, R. Essential roles of Notch signaling in maintenance of neural stem cells in developing and adult brains. *J. Neurosci.* **30**, 3489–3498 (2010).
24. Guillemot, F. Spatial and temporal specification of neural fates by transcription factor codes. *Development* **134**, 3771–3780 (2007).
25. Ladewig, J. et al. Small molecules enable highly efficient neuronal conversion of human fibroblasts. *Nat. Methods* **9**, 575–578 (2012).
26. Dias Moura Prazeres, P. H. et al. Pericytes are heterogeneous in their origin within the same tissue. *Dev. Biol.* **427**, 6–11 (2017).
27. La Manno, G. et al. Molecular diversity of midbrain development in mouse, human, and stem cells. *Cell* **167**, 566–580.e19 (2016).
28. Göritz, C. et al. A pericyte origin of spinal cord scar tissue. *Science* **333**, 238–242 (2011).
29. Chambers, S. M. et al. Highly efficient neural conversion of human ES and iPS cells by dual inhibition of SMAD signaling. *Nat. Biotechnol.* **27**, 275–280 (2009).
30. Liu, M. L. et al. Small molecules enable neurogenin 2 to efficiently convert human fibroblasts into cholinergic neurons. *Nat. Commun.* **4**, 2183 (2013).
31. Kageyama, R., Ohtsuka, T., Shimojo, H. & Imayoshi, I. Dynamic regulation of Notch signaling in neural progenitor cells. *Curr. Opin. Cell Biol.* **21**, 733–740 (2009).
32. Vasconcelos, F. F. et al. MyT1 counteracts the neural progenitor program to promote vertebrate neurogenesis. *Cell Rep.* **17**, 469–483 (2016).
33. Engler, A. et al. Notch2 signaling maintains NSC quiescence in the murine ventricular-subventricular zone. *Cell Rep.* **22**, 992–1002 (2018).
34. Radonjić, N. V. et al. Diversity of cortical interneurons in primates: the role of the dorsal proliferative niche. *Cell Rep.* **9**, 2139–2151 (2014).

Author contributions

M.K., J.G.C., B.T., and B.B. conceived the study and designed experiments; M.K. performed direct reprogramming experiments; M.K., S.F., A.P., and V.K.T. analyzed bulk RNA-seq data; A.B. helped with processing of the 10xGenomics data; A.G. performed RNA isolation for bulk RNA-seq analysis; W.F. performed time-lapse imaging experiments; T.R. performed electrophysiological recordings; A.C. performed Sholl analyses; A.S. performed immunocytochemical analyses; C.S. provided human brain biopsies; M.G. provided material; J.G.C., M.G.-S., and T.G. performed single-cell RNA-seq experiments and sequenced libraries; J.G.C., J.K., and B.T. analyzed single-cell RNA-seq data; all authors discussed the data; and M.K., J.G.C., S.F., B.T., and B.B. wrote the paper.

Competing interests

The authors declare no competing interests.

Additional information

Methods

Culture of primary human pericytes. Primary pericytes were derived as described previously from adult human brain tissue[16,35]. Briefly, specimens of cerebral cortex were obtained from standard surgical interventions of patients aged 19–70 years old and of both sexes. The study was approved by the ethical committee of the Medical Faculty of the LMU Munich, and written informed consent was obtained from all patients. Human tissue was enzymatically (TrypLE, Life technologies) and mechanically dissociated, and, following centrifugation at 1,000 rpm for 5 min and resuspension in pericyte medium, cells were plated in T75 cell-culture flasks. Pericyte growth medium consisted of DMEM high glucose with Glutamax, 20% FBS, and penicillin/streptomycin. Medium was changed twice per week and subcultivation at a ratio of 1:3 was performed every 10–14 d. Cells were grown under low-oxygen conditions (5% O_2, 5% CO_2; Galaxy 170R, New Brunswick).

Retroviral transduction and treatments of human pericytes. The retroviral backbone used for lineage conversion of pericytes into iNs allowed for the polycistronic expression of *Ascl1* and *Sox2* (connected via p2A) under the control of an internal chicken β-actin promoter with cytomegalovirus enhancer (CAG) together with either *DsRed* or *GFP* downstream of an internal ribosomal entry site (IRES). For control, cultures were transduced with a virus encoding only *DsRed* or *GFP* behind an IRES site as described previously[13,16].

Retroviral transduction of primary pericyte cultures was performed 24 h after plating on either poly-D-lysine-coated glass coverslips or in T25 or T75 cell-culture flasks without coating, using VSV-G (vesicular stomatitis virus glycoprotein)-pseudotyped retroviruses encoding neurogenic fate determinants as described previously[16,35]. Samples (pericyte donors, coverslips in 24-well plates or in T25 or T75 cell-culture flasks) were randomly assigned for transduction with different viruses. Twenty-four hours after transduction, the medium was replaced by a differentiation medium consisting of DMEM high glucose with Glutamax and B27 supplement (Gibco). For growth factor or small-molecule treatments, addition was performed 1, 3, and 5 d following transduction. Factors were added to a final concentration of 1 μM[30,36] for dorsomorphin (Sigma-Aldrich), 10 μM for DAPT (*N*-[*N*-(3,5-difluorophenacetyl)-L-alanyl]-*S*-phenylglycine *t*-butyl ester; Stem Cell Technologies), 10 μM[37,38] for SB431542 (Stem Cell Technologies), 30 ng/mL[39,40] for recombinant human BMP4 (Preprotech), and 1 μg/mL[41,42] for recombinant human NODAL (RnD Systems). Cells were allowed to differentiate under low-oxygen conditions (5% O_2, 5% CO_2). Reprogramming efficiency was calculated by quantifying TUBB3-immunoreactive cells among reporter-positive transduced cells 3–5 weeks following transduction with retroviruses.

Fluorescence-activated cell sorting (FACS). For sorting of transduced cells for further culturing, bulk RNA-sequencing, or scRNA-sequencing, primary pericytes were detached from the culture dish using TrypLE for 4–6 min and subsequently resuspended in 500–1,000 μL pericyte growth medium. Cell sorting was performed by taking advantage of the combined expression of Ascl1 and Sox2 with a fluorescent reporter protein (either DsRed or GFP). Gating was achieved via subtracting the autofluorescence of nontransduced cells; control (DsRed or GFP only)-transduced cells were used as respective controls. Following sorting, cells were (i) collected in pericyte growth medium and plated on PDL-coated glass cover slips on 24-well plates for further culturing, (ii) directly collected into RLT buffer (Qiagen) and stored at –80 °C until RNA isolation for bulk RNA-seq, or (iii) prepared for single-cell loading onto a C1 Fluidigm chip for scRNA-seq. To separate LEPR+ and LEPR- pericyte populations, pericyte cultures were detached from the culture dish using TrypLE for 4–6 min and subsequently 1×10^5–5×10^5 cells were resuspended in 100 μL staining solution (PBS plus 0.5% BSA). Primary antibody (Alexa Fluor 647-conjugated CD295 (anti-LEPR; 1:20, BD Pharmingen, cat.no. 564376) was added and cells were incubated for 30 min on ice in the dark. After washing three times in staining solution, cells were resuspended in 500 μL pericyte growth medium and subjected to cell sorting using a FACS Aria (BD). An Alexa Fluor 647-conjugated isotype control antibody (1:100, BD Pharmingen) was used to gate the proper populations.

Immunohistochemical staining. Cell cultures were fixed in 4% paraformaldehyde (PFA) in phosphate-buffered saline (PBS) for 15 min at room temperature. Cells were first pretreated in blocking solution consisting of 0.2–0.5% Triton X-100 and 10% donkey serum in PBS for 60 min, followed by incubation with the primary antibodies in 100 μL in the same solution for 1 h at room temperature (20–23 °C) or overnight at 4 °C. After extensive washing in PBS, cells were incubated in the same solution with appropriate species- or subclass-specific secondary antibodies conjugated to fluorophores. Coverslips were finally mounted onto a glass slide with an anti-fade mounting medium (Aqua Poly/Mount; Polysciences, Warrington, PA). For multidimensional immunofluorescence staining, fixed cell cultures were subjected to sequential immunofluorescence staining/destaining cycles adapted from a technique published by Schubert et al.[43].

Microscopy and time-lapse imaging. Immunocytochemical stainings were first examined with an epifluorescence microscope (BX61, Olympus) equipped with the appropriate filter sets. Stainings were further analyzed with a LSM710 laser-scanning confocal microscope (Carl Zeiss,). Digital images were captured using the ZEN software (Carl Zeiss).

We performed time-lapse microscopy to follow the reprogramming process of pericytes into iNs. Pericytes were transduced with Ascl1-Sox2-CAG-GFP retrovirus. Twenty-four hours after transduction, medium was replaced by a differentiation medium consisting of DMEM high glucose with Glutamax and B27 supplement (Gibco). The microwell plate containing these cells was 48 h later placed on a heated microscopic stage with 5% CO_2 and 37 °C and imaged continuously for up to 14 dys. Fluorescent images were taken subsequently once every 4 h and brightfield images once every 5 min. After completion of time-lapse imaging, cells were fixed with 4% PFA, and after imaging ICC was performed to corroborate the results from the imaging. Data analysis was performed using Timm's Tracking Tool (TTT) software.

Sholl analysis. Sholl analysis was performed by using the ImageJ plugin Sholl Analysis[44]. Confocal images of iNs with immunocytochemical stainings against TUBB3 were used for tracing individual neuronal processes of selected cells in ImageJ (Fiji) software[45]. After assigning the center of each cell soma, a grid with concentric circles with increasing diameter (5 μm) was superimposed. The data are expressed as the mean ± s.e.m. of the values obtained in four independent experiments; untreated $n = 14$, dorsomorphin-treated $n = 14$. The investigators carried out blinded analyses.

Neuromorphometry. Several parameters of cell morphology were examined. Neuronal complexity quantification was conducted with the following measurements: (i) primary branches, i.e., processes emerging directly from the soma per neuron; (ii) dendritic segment, i.e., part of the dendrite between two branching points; (iii) branching point, i.e., the point at the dendrite where a dendrite ramifies into two or more; (iv) maximum dendritic length or ending radius, i.e., the radius of the largest circle of the superimposed Sholl mask; (v) soma size (in μm²), i.e., cross sectional surface area of the cell body; and (vi) sum of intersections, i.e., the sum of all intersections between the dendritic arbors and the concentric circles radiating from the cell body. The numbers of primary branches, as well as the numbers of dendritic segments and branching points, were counted manually. ImageJ Fiji software was used to measure soma size. The sum of intersections and the ending radius were measured using the Sholl method (see "Sholl analysis" section, above).

Statistics. To test for statistical significance, two-tailed unpaired Student's *t* tests were used. Asterisks indicate statistically significant differences across the two groups: *$P < 0.05$, **$P < 0.01$, ***$P < 0.001$. The analyses were done using Prism (GraphPad) or R. Data distribution was assumed to be normal, but this was not formally tested. Throughout the study, boxplots show medians, quartiles (box), and ranges (whiskers). No statistical methods were used to predetermine sample sizes, but our sample sizes are similar to those reported in previous publications[11,16]. If not indicated otherwise, data collection and analysis were not performed blind to the conditions of the experiments. No data points were excluded from the analysis, except for cells in the scRNA-seq analyses that did not fulfill the required criteria (see below sections on scRNA-seq analyses).

Electrophysiology. For electrophysiological recordings, coverslips with reprogrammed cells were transferred to a recording chamber mounted on the stage of an upright microscope (Axioscope FS, Zeiss, Germany). Cells were perfused with a bathing solution consisting of (in mM): NaCl 150, KCl 3, CaCl2 3, MgCl₂ 2, HEPES 10, and D-glucose 10. The pH of the solution was adjusted to 7.4 (NaOH); the osmolarity ranged from 309 to 313 mOsmol. All recordings were performed at room temperature (23–24 °C). Electrodes for whole-cell patch-clamp recordings were fabricated from borosilicate glass capillaries (OD: 1.5 mm, ID: 0.86 mm; Hugo Sachs Elektronik-Harvard Apparatus) and filled with a solution composed of (in mM): potassium-gluconate 135, KCl 4, NaCl 2, EGTA 0.2, HEPES (potassium salt) 10, adenosine-triphosphate (magnesium salt, ATP[Mg]) 4, sodium guanosine-triphosphate (NaGTP) 0.5, and phosphocreatine 10 (pH: 7.25–7.30, osmolarity: 288–291 mOsmol). The electrodes (resistance: 5–7 MΩ) were connected to the headstage of a NPI ELC-03XS amplifier (NPI, Tamm, Germany). To visualize the cultured cells, the microscope was equipped with differential interference contrast (DIC) optics and with epifluorescence optics for green and red fluorescence (filter sets: Zeiss BP450-490, LP520, Zeiss BP546/12, lp590). Images were taken and displayed using a software-operated CCD microscope camera (ORCA R, Hamamatsu, Germany). Following membrane rupture, the cells were voltage-clamped to a holding potential of –60 mV and kept under this condition until the holding current stabilized (3–5 min). Then the amplifier was switched to current-clamp mode. The recorded signals were amplified (× 10), filtered at 10 or 20 kHz (current clamp) and at 5 kHz (voltage clamp), digitized at a sampling rate of 10 or 20 kHz and stored on a computer for offline analysis. Data acquisition and generation of command pulses was done using a CED 1401 Micro 3 system in conjunction with Signal6 data acquisition software (Cambridge electronic design). Data analysis was performed using IGOR Pro 6 (WaveMetrics, Lake Oswego, USA) together with the NeuroMatic IGOR plugin (www.neuromatic. thinkrandom.com). Determination of the input resistance, RN, was performed by

measuring the amplitude of a voltage deviation induced by a small hyperpolarizing current pulse (1 s, 2–10 pA). The total membrane capacity CN was estimated using a method described by Zemankovics et al.[46]. The ability of the cells to generate action potentials was tested by injecting depolarizing current pulses (50 ms) with increasing current strengths (ΔI: 2–10 pA) or by depolarizing current ramps (50 ms) from 0–100 pA. Spike discharge was analyzed by injecting a series of depolarizing current pulses (duration: 1 s) with a stepwise increment (ΔI: 2–10 pA).

Bulk RNA sequencing. Primary pericytes from three different human donors were transduced with Ascl1, Sox2, AS, and/or control retroviruses and purified by FACS at 2 and 7 dpi. RNA was isolated using the RNeasy Micro Kit (Qiagen). Following Ribo-Zero removal, the RNA-seq library was prepared in accordance with Illumina's instructions using oligo-dT primers. The RNA-seq output in FASTQ format was aligned to the human hg38 genome (sourced from UCSC) using TopHat v2.0.8[47] and only uniquely mapped reads were retained for further analysis. SAMTOOLS v.0.1.19[48] was used for file format conversions (SAM and BAM). The read counts per gene were calculated using HTSeq v0.5.4p1[49]. The DESeq package[50] was used thereafter for differential expression analysis. P_{adj} values were calculated with the Benjamini–Hochberg procedure.

GO terms analysis of bulk RNA-seq data. GO enrichment analysis was performed using the Bioconductor package TopGO employing the default algorithm weight01[51]. Genes were considered significantly deregulated with $P_{adj} < 0.01$. GO terms were ordered according to their significance as determined by Fisher's exact test.

Capture of single cells and preparation of cDNA. Transduced human brain pericytes were sorted using FACS and single cells were captured on a medium-sized (10- to 17-µm cell diameter) microfluidic RNA-seq chip using the Fluidigm C1 system. Cells were loaded onto the chip at a concentration of 350–500 cells per µL and imaged by phase-contrast to assess number of cells per capture site. Only single cells were included in the analysis. cDNAs were prepared on chip using the SMARTer v4 Ultra Input Low RNA kit for Illumina (Clontech).

RNA-seq library construction and cDNA sequencing. Size distribution and concentration of single-cell cDNA was assessed on a capillary electrophoresis-based fragment analyzer (Advanced Analytical Technologies), and only single cells with high quality cDNA were further processed. Sequencing libraries were constructed in 96-well plates using the Illumina Nextera XT DNA Sample Preparation kit, using primer sets A and B according to the protocol supplied by Fluidigm and as described previously[11]. Libraries were quantified by Agilent Bioanalyzer using a High Sensitivity DNA analysis kit, as well as fluorimetrically using Qubit dsDNA HS Assay kits and a Qubit 2.0 Fluorimeter (Invitrogen, Thermo Fisher Scientific). Up to 192 single-cell libraries were pooled and 100-bp paired-end sequenced on one lane of the Illumina HiSeq 2500 to a depth of at least 500,000 reads per cell. Base calling, adaptor trimming, and de-multiplexing was performed as described[52,53]. The transcriptomes of a total of 769 cells was measured from the following 12 independent experiments: 2-dpi control (76 cells, 1 experiment), 2-dpi Ascl1-only (82 cells, 1 experiment, 7-dpi Ascl1-only (64 cells, 1 experiment), 2-dpi AS (86 cells, 1 experiment), 7-dpi AS (48 cells, 1 experiment), 14-dpi AS (79 cells, 2 experiments), 21/22-dpi AS (130 cells, 2 experiments), 14-dpi ASD (183 cells, 2 experiments), and 14-dpi ASN (21 cells, 1 experiment). See Supplementary Table 5 for the transcriptome data for all 769 cells with annotations (quantification in $\log_2$(FPKM)).

Processing, analysis, and graphic display of single-cell RNA-seq data. Reads were aligned to a Bowtie2[54]-indexed human genome (hg38 sourced from Ensembl) supplemented with DNA sequences for *Egfp*, *mCherry*, *DsRed*, mouse *Ascl1*, and mouse *Sox2* using TopHat[47] with default settings. Transcript levels were quantified as fragments per kilobase of mapped reads (FPKM) generated by Cufflinks[55] using GENCODE protein-coding genes (hg38 Havana). We excluded cells that had less than 100,000 reads, expressed < 1,000 genes, or did not express either of two housekeeping genes *ACTB* and *GAPDH*. Transcript levels were converted to the log-space by taking the $\log_2$(FPKM). R studio (https://www.rstudio.com/) was used to run custom R scripts to perform PCA (FactoMineR package) and hierarchical clustering (stats package) and to construct heatmaps, correlation plots, scatter plots, violin plots, dendrograms, bar graphs, and histograms. Generally, ggplot2 and gplots packages were used to generate data graphs. The Seurat package implemented in R was used to identify cell clusters and perform differential gene expression based on t-SNE[56]. The Monocle2 package[20] was used to analyze cell lineage relationships. Covariance network analysis and visualizations were done using igraph implemented in R (http://igraph.org/). Signatures were calculated by summing the $\log_2$(FPKM) expression values of each gene in a set of genes comprising a signature (Supplementary Table 6).

10× Genomics scRNA-seq experiment. For the 10× Genomics experiment, cells were transfected with AS, treated with dorsomorphin, and analyzed at 14 dpi. Cells were sorted based on the expression of GFP and used for one encapsulation. 10× Genomics sample libraries were sequenced on an Illumina HiSeq 2500 and

base calling, adaptor trimming, and de-multiplexing of single cells were performed using 10× Genomics Cell Ranger 2.0 software. We performed PCA and t-SNE analyses using the Seurat v2.0 package for R on 3,419 single cells with 1,000–7,000 genes detected (Supplementary Table 7). We used genes correlating and anticorrelating with the first eight principal components to cluster the cells, and found that clustering patterns were robust across multiple PC inclusions. Neuronal cluster-specific markers were found using Seurat's implementation of the 'bimod' likelihood-ratio test for single-cell gene expression data, and the top genes were selected based on the average log fold-change.

Antibodies. The following antibodies were used: mouse (IgG2b) anti-TUBB3 (Sigma; cat. no. T8660; 1:300), rat IgG2a anti-CD49f-PE (Miltenyi Biotec; cat. no. 130-100-096; 1:11), recombinant human anti-CD4 (Miltenyi; cat. no. 130-109-537; 1:11), rabbit anti-GABA (Abcam; cat. no. ab17413; 1:1,000), chick anti-GFP (Aves; cat. no. GFP-1020; 1:500), mouse (IgG1) anti-Pvalb (Swant; cat. no. PV-235; 1:1,000), rabbit anti-Pdgfrb (Cell Signaling; cat. no. 3169S; 1:300), rat anti-RFP (Chromotek; cat. no. 5F8; 1:500), mouse (IgG2b) anti-SMA (Sigma; cat. no. A5228; 1:500), and rabbit anti-VGLUT1 (Synaptic Systems; cat. no. 135302; 1:500). For FACS we additionally used mouse (IgG2b) anti-LEPR Al647 (BD Pharmingen; cat. no. 564376; 1:20) and corresponding isotype control (BD Pharmingen; cat. no. 557903; 1:20). Antibodies were selected according to the antibody validation reported by the distributing companies.

Accession codes. GEO: scRNA-seq data, GSE113036.

Reporting Summary. Further information on experimental design is available in the Nature Research Reporting Summary linked to this article.

Data availability and accession codes. The scRNA-seq data used in this study have been deposited in the Gene Expression Omnibus (GEO) under accession number GSE113036. The data that support the findings of this study are available from the corresponding author upon reasonable request.

References

35. Karow, M., Schichor, C., Beckervordersandforth, R. & Berninger, B. Lineage-reprogramming of pericyte-derived cells of the adult human brain into induced neurons. *J. Vis. Exp.* https://doi.org/10.3791/51433 (2014).
36. Yu, P. B. et al. Dorsomorphin inhibits BMP signals required for embryogenesis and iron metabolism. *Nat. Chem. Biol.* **4**, 33–41 (2008).
37. Inman, G. J. et al. SB-431542 is a potent and specific inhibitor of transforming growth factor-beta superfamily type I activin receptor-like kinase (ALK) receptors ALK4, ALK5, and ALK7. *Mol. Pharmacol.* **62**, 65–74 (2002).
38. Laping, N. J. et al. Inhibition of transforming growth factor (TGF)-beta1-induced extracellular matrix with a novel inhibitor of the TGF-beta type I receptor kinase activity: SB-431542. *Mol. Pharmacol.* **62**, 58–64 (2002).
39. Martynoga, B. et al. Epigenomic enhancer annotation reveals a key role for NFIX in neural stem cell quiescence. *Genes Dev.* **27**, 1769–1786 (2013).
40. Graham, A., Francis-West, P., Brickell, P. & Lumsden, A. The signalling molecule BMP4 mediates apoptosis in the rhombencephalic neural crest. *Nature* **372**, 684–686 (1994).
41. Chen, A. E., Borowiak, M., Sherwood, R. I., Kweudjeu, A. & Melton, D. A. Functional evaluation of ES cell-derived endodermal populations reveals differences between Nodal and Activin A-guided differentiation. *Development* **140**, 675–686 (2013).
42. Kumar, A. et al. Nodal signaling uses activin and transforming growth factor-beta receptor-regulated Smads. *J. Biol. Chem.* **276**, 656–661 (2001).
43. Schubert, W. Multiple antigen-mapping microscopy of human tissue. in *Experta Medica: Advances in Analytical Cellular Patphology* (eds. Burger, G., Oberholzer, M. & Vooijs, G.P.) 97–98 (Elsevier, Amsterdam, 1990).
44. Ferreira, T. A. et al. Neuronal morphometry directly from bitmap images. *Nat. Methods* **11**, 982–984 (2014).
45. Schindelin, J. et al. Fiji: an open-source platform for biological-image analysis. *Nat. Methods* **9**, 676–682 (2012).
46. Zemankovics, R., Káli, S., Paulsen, O., Freund, T. F. & Hájos, N. Differences in subthreshold resonance of hippocampal pyramidal cells and interneurons: the role of h-current and passive membrane characteristics. *J. Physiol.* **588**, 2109–2132 (2010).
47. Trapnell, C., Pachter, L. & Salzberg, S. L. TopHat: discovering splice junctions with RNA-Seq. *Bioinformatics* **25**, 1105–1111 (2009).
48. Li, H. et al. The Sequence Alignment/Map format and SAMtools. *Bioinformatics* **25**, 2078–2079 (2009).
49. Anders, S., Pyl, P. T. & Huber, W. HTSeq–a Python framework to work with high-throughput sequencing data. *Bioinformatics* **31**, 166–169 (2015).
50. Oshlack, A., Robinson, M. D. & Young, M. D. From RNA-seq reads to differential expression results. *Genome Biol.* **11**, 220 (2010).
51. Alexa, A., Rahnenführer, J. & Lengauer, T. Improved scoring of functional groups from gene expression data by decorrelating GO graph structure. *Bioinformatics* **22**, 1600–1607 (2006).

52. Renaud, G., Kircher, M., Stenzel, U. & Kelso, J. freeIbis: an efficient basecaller with calibrated quality scores for Illumina sequencers. *Bioinformatics* **29**, 1208–1209 (2013).

53. Renaud, G., Stenzel, U., Maricic, T., Wiebe, V. & Kelso, J. deML: robust demultiplexing of Illumina sequences using a likelihood-based approach. *Bioinformatics* **31**, 770–772 (2015).

54. Langmead, B. & Salzberg, S. L. Fast gapped-read alignment with Bowtie 2. *Nat. Methods* **9**, 357–359 (2012).

55. Trapnell, C. et al. Transcript assembly and quantification by RNA-Seq reveals unannotated transcripts and isoform switching during cell differentiation. *Nat. Biotechnol.* **28**, 511–515 (2010).

56. Macosko, E. Z. et al. Highly parallel genome-wide expression profiling of individual cells using nanoliter droplets. *Cell* **161**, 1202–1214 (2015).

nature research

Corresponding author(s): Marisa Karow, Barbara Treutlein, Benedikt Berninger

Reporting Summary

Nature Research wishes to improve the reproducibility of the work that we publish. This form provides structure for consistency and transparency in reporting. For further information on Nature Research policies, see Authors & Referees and the Editorial Policy Checklist.

Statistical parameters

When statistical analyses are reported, confirm that the following items are present in the relevant location (e.g. figure legend, table legend, main text, or Methods section).

n/a	Confirmed	
☐	☒	The exact sample size (*n*) for each experimental group/condition, given as a discrete number and unit of measurement
☐	☒	An indication of whether measurements were taken from distinct samples or whether the same sample was measured repeatedly
☐	☒	The statistical test(s) used AND whether they are one- or two-sided *Only common tests should be described solely by name; describe more complex techniques in the Methods section.*
☒	☐	A description of all covariates tested
☐	☒	A description of any assumptions or corrections, such as tests of normality and adjustment for multiple comparisons
☐	☒	A full description of the statistics including central tendency (e.g. means) or other basic estimates (e.g. regression coefficient) AND variation (e.g. standard deviation) or associated estimates of uncertainty (e.g. confidence intervals)
☐	☒	For null hypothesis testing, the test statistic (e.g. *F*, *t*, *r*) with confidence intervals, effect sizes, degrees of freedom and *P* value noted *Give P values as exact values whenever suitable.*
☒	☐	For Bayesian analysis, information on the choice of priors and Markov chain Monte Carlo settings
☒	☐	For hierarchical and complex designs, identification of the appropriate level for tests and full reporting of outcomes
☒	☐	Estimates of effect sizes (e.g. Cohen's *d*, Pearson's *r*), indicating how they were calculated
☐	☒	Clearly defined error bars *State explicitly what error bars represent (e.g. SD, SE, CI)*

Our web collection on statistics for biologists may be useful.

Software and code

Policy information about availability of computer code

Data collection	For Sholl analyses images were analyzed using the ImageJ(v1.51a-1.51h) Plugin Sholl Analysis v3.6.4; tracing individual neuronal processes was performed using ImageJ software.
Data analysis	Details about data analysis and visualization are provided in the Online Methods section of the paper. The following versions were used: Bioconductor package TopGO v2.3.1 employing the default algorithm weight01, GraphPad Prism v6.01, Igor Pro6 6.0.3.0; Custom R packages were used:TopHat v2.0.8, SAMTOOLS v.0.1.19, HTSeq v0.5.4p1. DESeq2 v1.3.0, FactoMineR v1.34, Seurat v1.4, Monocle2 v2.6.4, igraph v1.2.1, Seurat v2.1-2.2

For manuscripts utilizing custom algorithms or software that are central to the research but not yet described in published literature, software must be made available to editors/reviewers upon request. We strongly encourage code deposition in a community repository (e.g. GitHub). See the Nature Research guidelines for submitting code & software for further information.

Data

Policy information about availability of data

All manuscripts must include a data availability statement. This statement should provide the following information, where applicable:

- Accession codes, unique identifiers, or web links for publicly available datasets
- A list of figures that have associated raw data
- A description of any restrictions on data availability

The scRNA-seq data used in this study have been in the Gene Expression Omnibus (GEO) under accession number GSE113036. The data that support the findings of this study are available from the corresponding author upon reasonable request. Correspondence and requests for materials and data should be addressed to M.K. (marisa.karow@med.uni-muenchen.de), and B.T. (barbara_treutlein@eva.mpg.de), and B.B. (berningb@uni-mainz.de).

Field-specific reporting

Please select the best fit for your research. If you are not sure, read the appropriate sections before making your selection.

☒ Life sciences   ☐ Behavioural & social sciences   ☐ Ecological, evolutionary & environmental sciences

For a reference copy of the document with all sections, see nature.com/authors/policies/ReportingSummary-flat.pdf

Life sciences study design

All studies must disclose on these points even when the disclosure is negative.

Sample size	No statistical methods were used to pre-determine sample sizes but our sample sizes are similar to those reported in previous publications (Karow et al., Cell Stem Cell 2012; Treutlein et al., Nature 2016)
Data exclusions	No data points were excluded for the analysis, except for cells in the scRNA-seq analyses not fulfilling the required criteria. For the fluidigm C1 scRNA-seq data: We excluded cells that had less than 100,000 reads, did not express > 1000 genes, or did not express either of two housekeeping genes ACTB and GAPDH. For the 10x Genomics scRNA-seq data: only single cells with 1,000-7,000 genes were included; cells with lower or higher number of detected genes were excluded.
Replication	For all experiments all replicates are indicated in the figure legends or the methods sections. We have provided all informations to reproduce the experiments. All replications were successful.
Randomization	Samples (pericyte donors, coverslips in 24-well plates, T25 or T75 cell culture flasks) were randomly assigned for transduction with different viruses.
Blinding	scRNA-sequencing analyses were performed unbiasedly and therefore blinding is not applicable. Regarding all other data, if not indicated otherwise (e.g. Sholl analysis), data collection and analysis were not performed blind to the conditions of the experiments. These experiments were performed by a single experimentator (MK)

Reporting for specific materials, systems and methods

Materials & experimental systems

n/a	Involved in the study
☐	☒ Unique biological materials
☐	☒ Antibodies
☐	☐ Eukaryotic cell lines
☐	☐ Palaeontology
☐	☐ Animals and other organisms
☐	☒ Human research participants

Methods

n/a	Involved in the study
☐	☐ ChIP-seq
☐	☒ Flow cytometry
☐	☐ MRI-based neuroimaging

Unique biological materials

Policy information about availability of materials

Obtaining unique materials	All unique material (Ascl1/Sox2 encoding viruses) are available from the authors upon

Obtaining unique materials	reasonable request. Any other material is published elsewhere or commercially available.

Antibodies

Antibodies used	Mouse (IgG2b) anti-TUBB3 (Sigma; cat.no. T8660; 1:300), rat IgG2a anti-CD49f-PE (Miltenyi Biotec; cat.no. 130-100-096; 1:11), recombinant human anti-CD4 (Miltenyi; cat.no. 130-109-537; 1:11), rabbit anti-GABA (Abcam; cat.no. ab17413; 1:1000), chick anti-GFP (Aves; cat.no. GFP-1020; 1:500), mouse (IgG1) anti-Pvalb (Swant; cat.no. PV-235; 1:1000), rabbit anti-Pdgfrb (Cell Signaling; cat.no. 3169S; 1:300), rat anti-RFP (Chromotek; cat.no. 5F8; 1:500), mouse (IgG2b) anti-SMA (Sigma; cat.no. A5228; 1:500), rabbit anti-VGLUT1 (Synaptic Systems, cat.no. 135302; 1:500). For FACS: mouse (IgG2b) anti-LEPR Al647 (BD Pharmingen; cat.no. 564376; 1:20), corresponding isotype control (BD Pharmingen; cat.no. 557903; 1:20).
Validation	Antibodies were selected according to the antibody validation reported by the distributing companies.

Eukaryotic cell lines

Policy information about cell lines

Cell line source(s)	no eukaryotic cell lines used
Authentication	no eukaryotic cell lines used
Mycoplasma contamination	no eukaryotic cell lines used
Commonly misidentified lines (See ICLAC register)	no eukaryotic cell lines used

Palaeontology

Specimen provenance	no specimen used
Specimen deposition	no specimen used
Dating methods	no specimen used

☐ Tick this box to confirm that the raw and calibrated dates are available in the paper or in Supplementary Information.

Animals and other organisms

Policy information about studies involving animals; ARRIVE guidelines recommended for reporting animal research

Laboratory animals	no animals or other organisms used
Wild animals	no animals or other organisms used
Field-collected samples	no animals or other organisms used

Human research participants

Policy information about studies involving human research participants

Population characteristics	no human research participants
Recruitment	no human research participants

ChIP-seq

Data deposition

☐ Confirm that both raw and final processed data have been deposited in a public database such as GEO.

☐ Confirm that you have deposited or provided access to graph files (e.g. BED files) for the called peaks.

| Data access links
May remain private before publication.	no ChiP-seq data included in this study
Files in database submission	*Provide a list of all files available in the database submission.*
Genome browser session (e.g. UCSC)	*Provide a link to an anonymized genome browser session for "Initial submission" and "Revised version" documents only, to enable peer review. Write "no longer applicable" for "Final submission" documents.*

Methodology

Replicates	*Describe the experimental replicates, specifying number, type and replicate agreement.*
Sequencing depth	*Describe the sequencing depth for each experiment, providing the total number of reads, uniquely mapped reads, length of reads and whether they were paired- or single-end.*
Antibodies	*Describe the antibodies used for the ChIP-seq experiments; as applicable, provide supplier name, catalog number, clone name, and lot number.*
Peak calling parameters	*Specify the command line program and parameters used for read mapping and peak calling, including the ChIP, control and index files used.*
Data quality	*Describe the methods used to ensure data quality in full detail, including how many peaks are at FDR 5% and above 5-fold enrichment.*
Software	*Describe the software used to collect and analyze the ChIP-seq data. For custom code that has been deposited into a community repository, provide accession details.*

Flow Cytometry

Plots

Confirm that:

☐ The axis labels state the marker and fluorochrome used (e.g. CD4-FITC).

☒ The axis scales are clearly visible. Include numbers along axes only for bottom left plot of group (a 'group' is an analysis of identical markers).

☒ All plots are contour plots with outliers or pseudocolor plots.

☐ A numerical value for number of cells or percentage (with statistics) is provided.

Methodology

Sample preparation	For sorting of transduced cells for further i) culturing, ii) bulk RNA-sequencing, iii) scRNA-sequencing, primary pericytes were detached from the culture dish using TrypLE for 4-6 minutes and subsequently resuspended in 500-1000 µl pericyte growth medium. For the separation of LEPR-positive and -negative pericyte populations, pericyte cultures were detached from the culture dish using TrypLE for 4-6 minutes and subsequently 1-5 x 105 cells were resuspended in 100 µl staining solution (PBS plus 0.5% BSA).
Instrument	FACS Aria (BD)
Software	FACS Diva Software
Cell population abundance	The purity of the fluorescent reporter-positive populations that were used for (bulk- and) scRNA-sequencing was confirmed via quantification of the reporter gene expression and resulted in a purity of more than 92%. Due to limitations of using the directly PE conjugated anti-LepR antibody, the purity of the post-sort fraction of the LepR-positive cell population could not be confirmed by additional post-FACS immunohistochemistry.
Gating strategy	For sort of transduced cells: Gating was achieved via subtracting the autofluorescence of non transduced cells and control (DsRed or GFP only) transduced cells were used as respective controls. For the LEPR-based sort: An Alexa647-conjugated isotype control antibody (1:100, BD Pharmingen) was used to gate the proper populations.

☒ Tick this box to confirm that a figure exemplifying the gating strategy is provided in the Supplementary Information.

Magnetic resonance imaging

Experimental design

Design type	no MRI imaging used in this study
Design specifications	*Specify the number of blocks, trials or experimental units per session and/or subject, and specify the length of each trial or block (if trials are blocked) and interval between trials.*
Behavioral performance measures	*State number and/or type of variables recorded (e.g. correct button press, response time) and what statistics were used to establish that the subjects were performing the task as expected (e.g. mean, range, and/or standard deviation across subjects).*

Acquisition

Imaging type(s)	*Specify: functional, structural, diffusion, perfusion.*
Field strength	*Specify in Tesla*
Sequence & imaging parameters	*Specify the pulse sequence type (gradient echo, spin echo, etc.), imaging type (EPI, spiral, etc.), field of view, matrix size, slice thickness, orientation and TE/TR/flip angle.*
Area of acquisition	*State whether a whole brain scan was used OR define the area of acquisition, describing how the region was determined.*

Diffusion MRI ☐ Used ☐ Not used

Preprocessing

Preprocessing software	*Provide detail on software version and revision number and on specific parameters (model/functions, brain extraction, segmentation, smoothing kernel size, etc.).*
Normalization	*If data were normalized/standardized, describe the approach(es): specify linear or non-linear and define image types used for transformation OR indicate that data were not normalized and explain rationale for lack of normalization.*
Normalization template	*Describe the template used for normalization/transformation, specifying subject space or group standardized space (e.g. original Talairach, MNI305, ICBM152) OR indicate that the data were not normalized.*
Noise and artifact removal	*Describe your procedure(s) for artifact and structured noise removal, specifying motion parameters, tissue signals and physiological signals (heart rate, respiration).*
Volume censoring	*Define your software and/or method and criteria for volume censoring, and state the extent of such censoring.*

Statistical modeling & inference

Model type and settings	*Specify type (mass univariate, multivariate, RSA, predictive, etc.) and describe essential details of the model at the first and second levels (e.g. fixed, random or mixed effects; drift or auto-correlation).*
Effect(s) tested	*Define precise effect in terms of the task or stimulus conditions instead of psychological concepts and indicate whether ANOVA or factorial designs were used.*

Specify type of analysis: ☐ Whole brain ☐ ROI-based ☐ Both

Statistic type for inference (See Eklund et al. 2016)	*Specify voxel-wise or cluster-wise and report all relevant parameters for cluster-wise methods.*
Correction	*Describe the type of correction and how it is obtained for multiple comparisons (e.g. FWE, FDR, permutation or Monte Carlo).*

Models & analysis

n/a	Involved in the study
☐	☐ Functional and/or effective connectivity
☐	☐ Graph analysis
☐	☐ Multivariate modeling or predictive analysis

Functional and/or effective connectivity	*Report the measures of dependence used and the model details (e.g. Pearson correlation, partial correlation, mutual information).*
Graph analysis	*Report the dependent variable and connectivity measure, specifying weighted graph or binarized graph, subject- or group-level, and the global and/or node summaries used (e.g. clustering coefficient, efficiency, etc.).*
Multivariate modeling and predictive analysis	*Specify independent variables, features extraction and dimension reduction, model, training and evaluation metrics.*